Proceedings of the 2006 IEEE International Conference on Robotics and Automation
Orlando, Florida - May 2006

Optical Torque Sensors for Implementation of Local Impedance Control of the Arm of Humanoid Robot

Dzmitry Tsetserukou[1], Riichiro Tadakuma[2], Hiroyuki Kajimoto[1] and Susumu Tachi[2]
Graduate School of Information Science and Technology
The University of Tokyo
7-3-1 Hongo, Bunkyo-ku, Tokyo 113-8656, Japan
[1]{dima_teterukov, hiroyuki_kajimoto}@ipc.i.u-tokyo.ac.jp, [2]{tadakuma, tachi}@star.t.u-tokyo.ac.jp

***Abstract* - This paper describes the recent development of new optical torque sensor in order to replace expensive strain gauge sensor attached at the tip of the anthropomorphic robot arm and realize local impedance control in each joint.**

Index Terms - Optical torque sensor, Impedance control.

I. Introduction

The teleoperated slave robot has been developed to realize dexterous tasks such as interaction with human in remote environment or manipulation with objects in hazardous conditions [1]. The slave robot includes anthropomorphic seven-degree of freedom (7-DOF) arms (Fig. 1) with 8-DOF hands. To achieve the stability in contact with environment and to realize controlled dynamic interaction between a robot arm and human the impedance control has been successfully applied. The impedance control of the arm of the remote slave robot requires measurement of external force exerted by human during interaction. The force imparted by human at the tip of the anthropomorphic arm is measured by 6-axis force sensor (MINI 4/20, BL AUTOTEC), marked by yellow rectangles in Fig. 1.

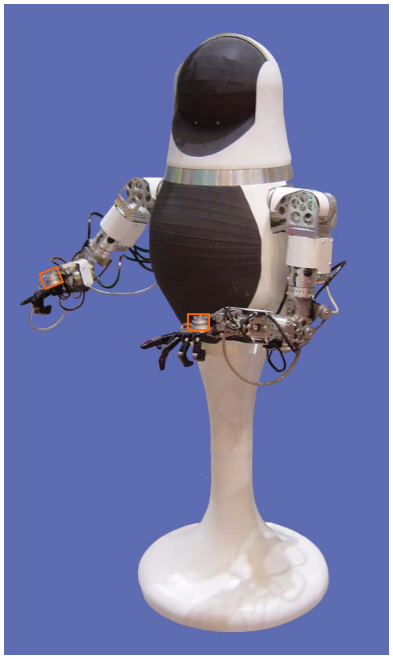

Fig. 1 Teleoperated slave robot.

In spite of the fact that developed robotic system ensures the safety in the interaction at the end-effector, other parts of the mechanical structure, such as shoulder and elbow joint, during operation can hurt people. In these joints there are no force measurement sensors to limit the motor torque by means feedback. Direct sensing of the applied torque through the value of current in DC motor circuit is unacceptable due to low backdrivability of the harmonic drives with high gear ratio (=50). Therefore, to realize human friendly interaction of any part of the anthropomorphic arm we decided to attach torque sensor at each joint to implement local impedance control. Thus, virtual backdrivability of transmissions can be achieved in each joint of the slave robot.

Besides, commercial 6-axis strain-gauge-based force/torque sensors are intended for use at the end-effector of a robot to monitor assembly or machining forces. In this application very high stiffness is required. However, for human-robot interaction high stiffness is not the objective. Moreover, strain gauges have many disadvantages: difficult to install, calibrate, easy to break and posses high electrical noise sensitivity that makes them rather expensive.

The authors introduce the idea of using optical approach to detect torque and discuss the results of realization of the local impedance control on the base of developed optical sensors to provide safety of human-robot interaction.

II. Methods of Torque Measurement. Advantages and Drawbacks

Torque transducer is attached to the motor shaft and includes load cell – structure which supports the load and deflects a known amount in response to applied torque. To measure the deformation of the flexure different approaches can be used. The primary methods are as follows:

1) *Electrical methods.*
2) *Methods based on electromagnetic phenomena.*
3) *Optical methods.*

Within these approaches noncontact transducers measuring relative displacement by means light radiation detection, Hall effect, Faraday`s law and contacting ones measuring strain based on strain gauges, potentiometers, piezoceramics and optical fibre are recognized.

Electrical measuring methods are associated essentially with strain gauges, capacitive and piezoelectric sensing. The operation of strain gauges is based on phenomena of the variation of their electrical resistance with strain. When force is applied the strain changes the electrical resistance of the gauges in proportion to the load. In spite of such benefits of strain gauges as high accuracy (linearity), about 0.03%-2.5% of full scale (FS), high resolution of 1-3mV/V, their maximum allowable strain is close at which they break. To guarantee the overload protection of transducer the mechanical stops limiting the deflections of the flexures are necessary. Very stiff sensor may only deflect a few ten-thousandths of

millimetre. Manufacturing the limit stops with such small clearances is very difficult. Besides, strain-gauge-based torque/force sensors are greatly subjected by radial and other force components. Semiconductor as well as foil gages require elaborate process for attachment which must be done by a specialist. Another shortcoming of these sensors is their sensitivity to electrical noise and temperature [2].

Many torque transducers are based on measuring the relative angle between the two ends of the torsion bar. This principle was realized in differential capacitive sensor for measuring the relative angle [3]. Developed transducer is noncontact, robust and compact. Two rotatable electrodes are placed between two sensor plates. The relative angle between the two rotors and the absolute position of the rotor blades are calculated from measurement of capacitive coupling between different transmitting stator segment and a single receiving electrode. Its drawback is high sensitivity to a radial displacement and high cost. The relationship between value of capacitor capacity and permittivity of the dielectric material between the capacitor plates also was used in patent [4].

In electromagnetic sensors the Faraday`s law (inductive sensors), magnetostriction and magnetoelastic effect are employed. As example of electromagnetic sensors – Linear Variable Differential Transformers (LVDT) have high degree of robustness, remarkable resolution of about 0.1μm, good accuracy (0.01-0.3%), allow easier installation and calibration. Inductive sensors suffer a reduction in signal at very low frequencies and affected by electromagnetic noise.

Light source, photosensor and solid object modifying amount of light incident on optical detector are necessary to measure displacement between unmovable and flexible part of the optical sensor. The photosensors have such drawbacks as nonlinearity and temperature sensitivity, however, they are considerably more reliable, cheap and allow simplifying the construction of the design. A displacement can be detected by interrupting light between source and detector, changing the intensity of reflected light or relative movement of source and detector. S. Hirose and K. Yoneda have made significant contribution to research of the optical force and moment sensors [5, 6]. The authors proposed to use a split type photosensor to detect the displacement of the light source (LED) caused by applied force in two directions. In cooperation with Minebea Co. OPFT series of 6-axes optical torque sensors was manufactured. In comparison with conventional strain-gauge-based transducers they are more compact, light in weight and low in cost. However, these sensors suffer from complicated calibration procedure due to nonlinear output, require application of DSP for real-time computation of measured force and have average accuracy of 5% FS. The idea of the patent [7] is calculating torque by measuring angle of twist of the torsion shaft through detection of difference in the rotation position of discs attached at the opposite sides of the torsion shaft using optical encoder. Encoder type of torque sensor suffers from large overall dimension and complicated procedure of apertured discs mounting. To overcome this the author [8] invented torque sensor including a source of optical radiation, a two dimensional array of radiation detector and two modulating apertured discs placed between source and detector. As torque applied to the shaft the relative position between discs alters overlapping slots and hence the size of the apertures which control the pattern of light incident upon the optical detector.

III. Development of the Optical Torque Sensor

Above-mentioned sensors have not been adapted to application in robot for torque detection. The approach to design high-performance torque sensor for anthropomorphic robot arm should follow the guidelines illustrated below.

1. Addition of the torque sensor to a robot joint should not require redesign of the joint and causes a minimal modification in kinematics and dynamics. Therefore, sensor with small width and lightweight is desirable.
2. Noise created by current passing through the DC motor attached in each joint of the robot arm should not effect considerably on sensing element. Hence, usage of electromagnetic sensors should be avoided in this application.
3. The angle of twist of the movable part of transducer at the maximum expected external torque should allow exploiting as wide range of detector sensitivity as possible to achieve high signal-to-noise ratio.
4. Torsional stiffness of the sensor should not considerably reduce the natural frequency of the robot arm. This introduces the trade-off of stiffness maximization while maintaining high sensitivity.
5. The other difficulty in design of the torque sensor is hysteresis elimination. Most metals used as flexures have very little hysteresis. However, bolted, press fit and welded joints near the flexure introduce hysteresis. Therefore, the optimal design requires realization of the mechanical structure from a single piece of metal.
6. Influence from any of the non-torsional components of the load should be canceled. Behavior of the sensing element output and mechanical structure should be as close to linear as possible.
7. Simple to manufacture, low in cost and robust.

We decided to use ultra-small size photointerrupters type RPI-131 and RPI-121 as sensitive element to measure relative motion of sensor's component. The relationship between the output signal and position of the shield plate for RPI-121 is shown in Fig. 2 [9].

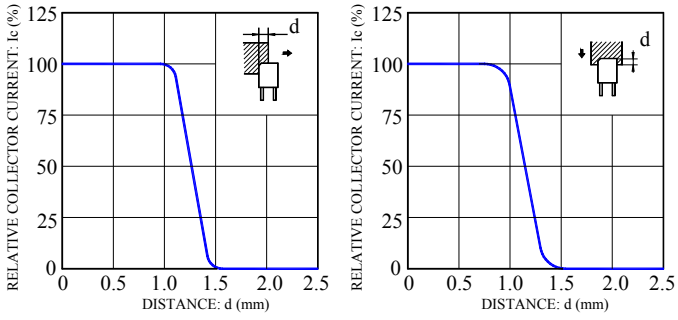

Fig. 2 Relative output vs. distance.

The linear section of the diagram corresponding approximately 0.2 mm can be used for detection of the relative displacement of the object. The dimensions of photointerrupter (RPI-121 3.6 × 2.6 × 3.3 mm) and weight of 0.05 g allow realization of compact sensor design.

Two structures of elastic element were realized: the in-line structure – when the input and output section of the detector are displaced in axial direction by the torsion component. And the "in plane" one – when input and output of the sensor are disposed in one plane and linked by the bending radial flexures. The layout of the in-line structure on the basis of spring with cross-shaped cross section is presented in Fig. 3.

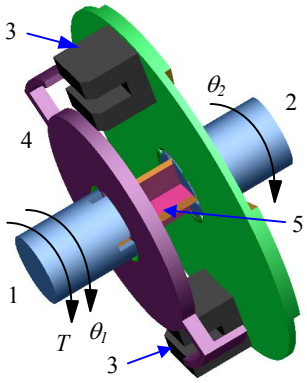

Fig. 3 Construction of the optical torque sensor.

This type of spring allows large deflections without yielding. Detector consists of input part 1, output part 2, fixedly mounted photointerrupters 3, shield 4 and spring 5. When torque T is applied to the input shaft the spring will be deflected. This causes rotation motion of the shield 4. The shield displacement is detected by the degree of interruption of infrared light falls on the phototransistor. Thus, magnitude of the output signal of the photointerrupter will correspond to the applied torque. The relationship between the sensed torque T_S and the angle of twist θ is the following:

$$T_S = k_S\theta = k_S\left(\theta_1 - \theta_2\right), \quad (1)$$

where k_S – torsional stiffness of the cross-shaped spring.

The cross-shaped spring behavior is similar to the equivalent flat plate behavior with some linear factor differences [10]. The torsional stiffness is defined as:

$$k_S = 0.98\left(b+h\right)t^3G/3l\,. \quad (2)$$

Here l, b, h, t – working length, width, height and thickness of the cross-shaped spring correspondingly, G – shear modulus. As far as angle of twist is very small it can be calculated from the displacement of the shield in tangential direction Δx, then (1) becomes:

$$T_S = k_S\,\Delta x/R_S\,. \quad (3)$$

Where R_S – distance from the sensor center to the middle of the shield plate in radial direction. The cross-shaped spring made from one piece of brass (G=3.7·10^{10} N/m^2, l = 12 mm, b = 10 mm, h = 10 mm, t = 1.5 mm is shown in Fig. 4.

Fig. 4 Cross-shaped spring.

The sensor was designed to withstand torque of 1.75 Nm. The results of spring analysis using Finite Element Method (FEM) show tangential displacement in mm (Fig. 5a) and von Mises stress in MPa (Fig. 5b) under torque of 1.75 Nm. The maximum value of von Mises stress equals $\sigma_{vonMises}$ = 2.392·10^8 N/m^2 <σ_{yield} = 2.4·10^8 N/m^2. Angle of twist can be calculated from the value of tangential displacement and for given load it equals 0.928°. Since the maximum stress appears in the area of core of the sensor the improvement of the design can be achieved by realization of hollow structure with 6 or 8 leaves of spring. The structure of the test rig for calibration of the optical sensor is given on three-dimensional model (Fig. 6).

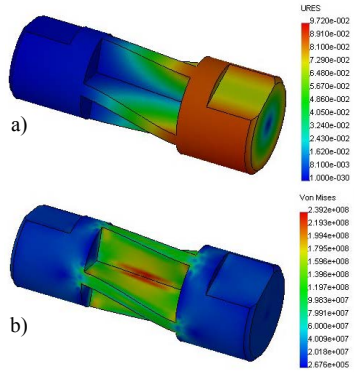

Fig. 5 Result of analysis using FEM.

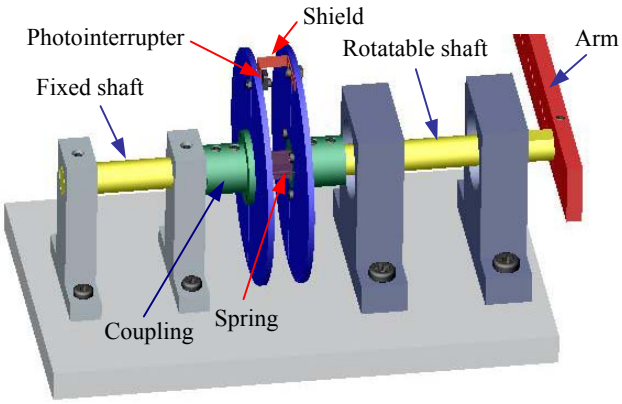

Fig. 6 Structure of the test rig.

Manufactured prototype of the test rig with electrical circuit is shown in Fig. 7.

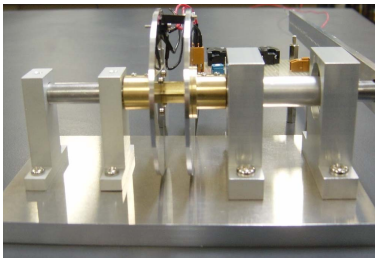

Fig. 7 Test rig.

Force applied to the arm, secured by screw to the rotatable shaft, creates the torque. Calibration was realized by means incrementation of angle of twist with small step and measuring output signal from the photointerrupter. Obtained relationship on linear section of transformation of displacement to voltage is shown in Fig. 8. This diagram can be rebuilt in term of applied torque, since torsional stiffness is known.

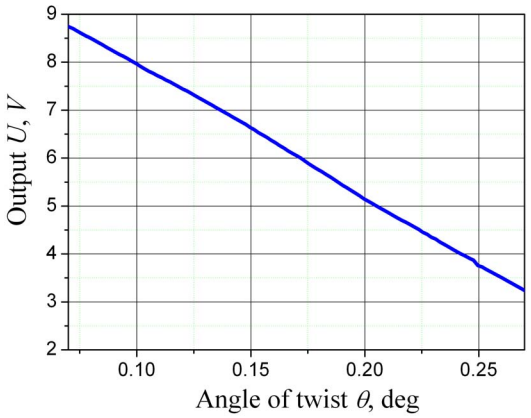

Fig. 8 Relationship of output voltage vs. angle of twist.

The "in plane" structure of the optical torque sensor includes the radial flexures subjected by loading bending forces while loading state. The layout of three-beam-hub-spoke structure is presented in Fig. 9.

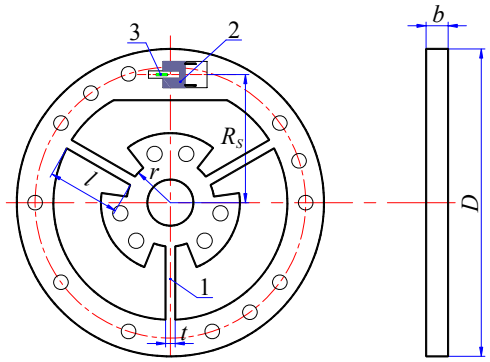

Fig. 9 Hub-spoke structure layout.

In Fig. 9 the following designations are given: 1 – beam, 2 – photointerrupter, 3 – shield. The rigidity of the hub can be increased by introducing additional evenly distributed spokes [11]. The torsional stiffness of hub-spoke structure is derived from:

$$k_S = 4NEI\left(\frac{1}{l}+\frac{3r}{l^2}+\frac{3r^2}{l^3}\right), \tag{4}$$

where N – number of spokes, l – the spoke length, E – modulus of elasticity, r – inner radius of the sensor [12]. Moment of inertia of the spoke cross section I can be calculated as:

$$I = \frac{bt^3}{12}, \tag{5}$$

here b – beam width, t – beam thickness. The sensor was designed to support of 0.8 Nm torque which arises in the elbow joint of the robot arm. The results of analysis using FEM show von Mises stress in MPa (Fig. 10a) and the tangential displacement in mm (Fig. 10b) under torque of 0.8 Nm. The maximum value of von Mises stress equals $\sigma_{vonMises}$ = $14.57 \cdot 10^7$ N/m^2 $< \sigma_{yield} = 15.0 \cdot 10^7$ N/m^2.

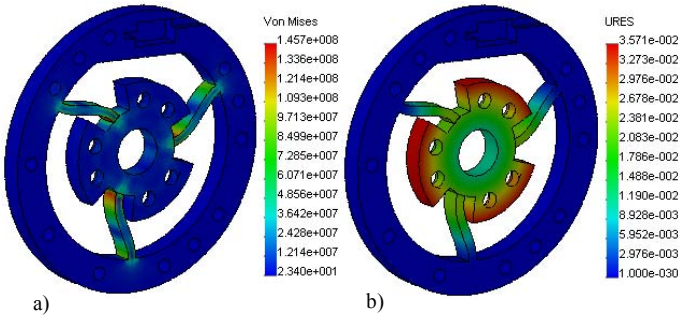

Fig. 10 Result of analysis of hub-spoke spring using FEM.

The test rig for calibration of the optical sensor has been created (Fig.11). The procedure of calibration is the same as previous sensor.

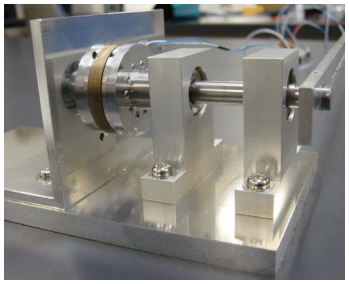

Fig. 11 Test rig.

Obtained relationship between angle of twist and output voltage is shown in Fig. 12.

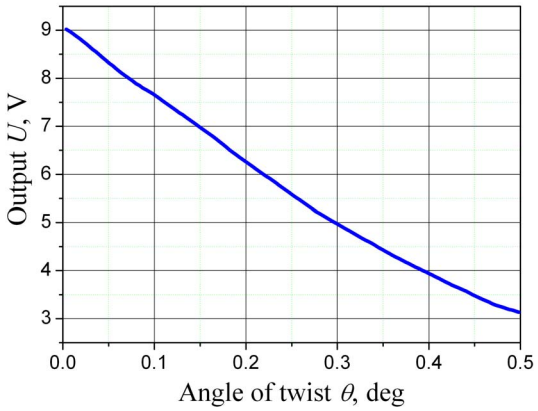

Fig. 12 Calibration result.

The sensor was manufactured from one piece of brass by using wire electrical discharge machining (EDM) cutting to eliminate hysteresis and guarantee high strength (Fig.13).

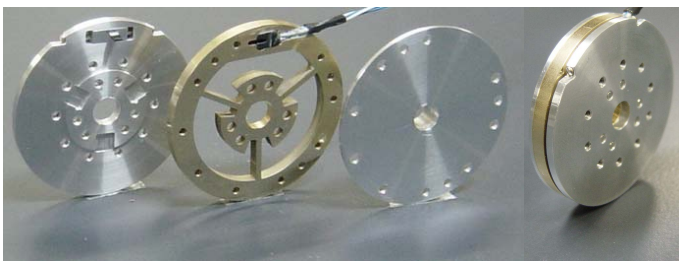

Fig. 13 Optical torque sensor with hub-spoke-shaped flexure.

In this sensor the photointerrupter type RPI-121 was used. The thickness of the sensor body is only 6.5 mm. The adjustment of the shield position is realized by rotation of oppositely located screws. The pitch of the screws is enough for smooth movement of the slider with shield plate.

In order to extend exploiting range of photodetector sensitivity keeping same strength the ring-shaped spring was designed. Components and assembly of the developed optical torque sensor are presented in Fig. 14. The flexible ring is connected with inner and outer part of the sensor though beams. The inner and outer beams are displaced with angle of 90° that enables large compliance of the ring-shaped flexure.

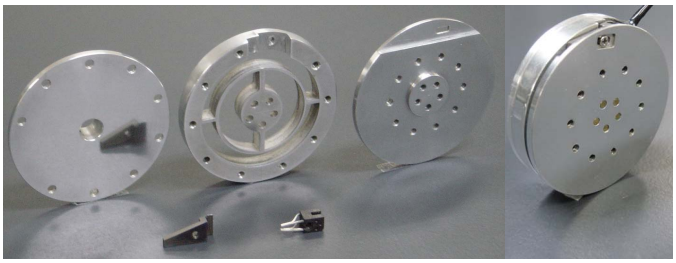

Fig. 14 Optical torque sensor with ring-shaped flexure.

The results of analysis using FEM under torque of 0.8 Nm are given in Fig. 14 (a – von Mises stress in MPa; b – tangential displacement in mm). The maximum value of stress equals $\sigma_{vonMises} = 8.62 \cdot 10^7$ N/m^2 < $\sigma_{yield} = 8.96 \cdot 10^7$ N/m^2.

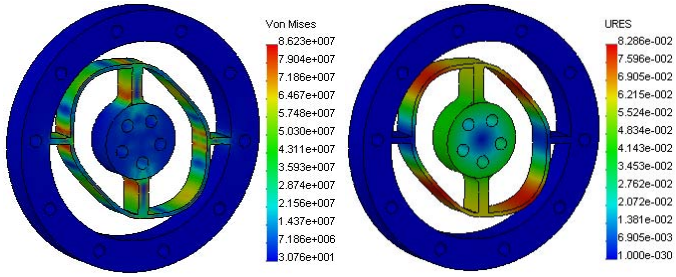

a) b)

Fig. 15 Result of analysis of the ring-shaped spring using FEM.

Obtained relationship between angle of twist θ and the output voltage of photointerrupter is shown in Fig. 16.

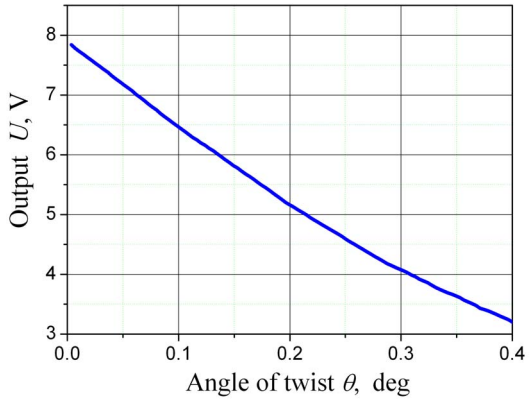

Fig. 16 Calibration result.

The thickness of the sensor is 10 mm. Displacement of the shield is measured by photointerrupter type RPI-131. The shortcomings of this design are complicated procedure of adjusting the position of the shield relatively photosensor and deficiency of the housing to prevent from damage of the optical transducer. Technical specification of the realized optical torque sensors is listed in Table I.

TABLE I
TECHNICAL SPECIFICATION

Type of sensor	Cross-shaped spring	Hub-spoke-shaped spring	Ring-shaped spring
Spring material	Brass C2801	Brass C2801	Aluminium A5052
Load capacity, Nm	1.75	0.8	0.8
Torsional stiffness, Nm/rad	90.02	219.8	115.9
Factor of safety	1.0	1.0	1.0
Photointerrupter type	RPI-131	RPI-121	RPI-131
Outer diameter, mm	30	42	42
Thickness, mm	30	6.5	10
Sensor mass, g	36	34.7	28.7

Cross-shaped spring provides transmission of large torque and small outer diameter of the sensor. However, this spring introduces considerable angle error caused significant compliance. Spoke-hub topology allows realization of compact in axial direction sensor. However, big torsional stiffness diminishes resolution of photointerrupter. Probably, the optimal solution is the ring-shaped flexure providing wide range of torsional stiffness with high mechanical strength. The main shortcoming of this topology is high sensitivity to the bending moment. Nevertheless, this obstacle can be overcome trough realization of simple supported loading shaft of the robot joint. In the most loaded joints, e.g. shoulder joint, such material as hardened stainless steel can be used for elastic element to keep the sensor dimension.

IV. LOCAL IMPEDANCE CONTROL

The aim of the impedance control is to establish the dynamic relationship between position error and force error in interaction similar to Newton`s second low of motion. The graphical presentation of concept of the local impedance control is given in Fig. 17.

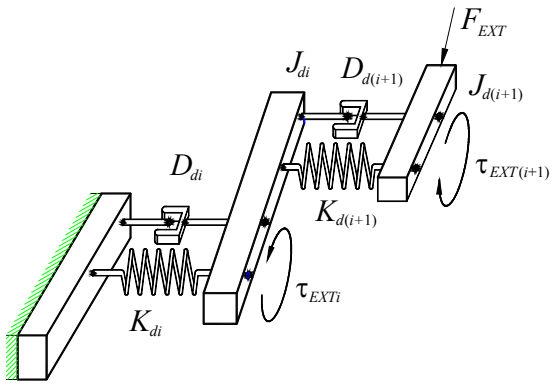

Fig. 17 Concept of the local impedance control.

In joint space system desired dynamics of robot joint *i* is:

$$\tau_{EXTi} = J_{di}\Delta\ddot{\theta}_i + D_{di}\Delta\dot{\theta}_i + K_{di}\Delta\theta_i;\ \Delta\theta_i = \theta_{ci} - \theta_{di}, \quad (6)$$

here τ_{EXTi} – torque applied to joint *i* caused by external force F_{EXT}, J_{di} – desired inertia, D_{di} – desired damping, K_{di} – desired stiffness, θ_{ci} – output joint angle of the impedance model, θ_{di} – desired joint angle. The state-space presentation of the equation of local impedance control can be written:

$$\begin{bmatrix}\Delta\dot{\theta}_i \\ \dot{v}_i\end{bmatrix} = \begin{bmatrix}0 & 1 \\ -K_d/J_d & -D_d/J_d\end{bmatrix}\begin{bmatrix}\theta_i \\ v_i\end{bmatrix} + \begin{bmatrix}0 \\ 1/J_d\end{bmatrix}\tau_{EXTi}(t). \quad (7)$$

Where state variable is defined as $v_i = \Delta\dot{\theta}_i$.

After integration of (7) the discrete time presentation of impedance equation can be expressed as:

$$\begin{bmatrix}\Delta\theta_{k+1} \\ \Delta\dot{\theta}_{k+1}\end{bmatrix} = A_d\begin{bmatrix}\Delta\theta_k \\ \Delta\dot{\theta}_k\end{bmatrix} + B_d T_{EXT(k)}. \quad (8)$$

Where A_d and B_d – matrixes mapped by discretization. In order to verify the dynamic behavior of the optical torque sensor the local impedance control of links of simple SCARA type manipulator was implemented (Fig.18, torque sensors are marked by ovals, gear ratio of speed reducers equals 2548).

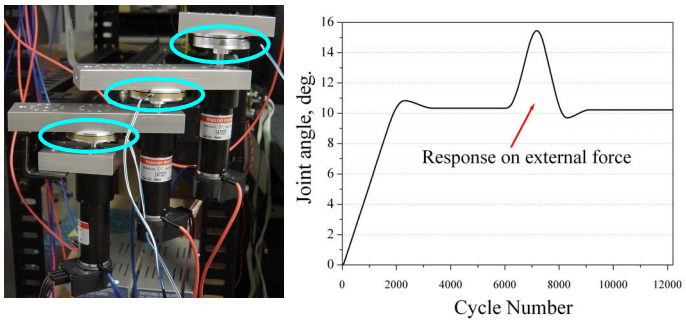

Fig. 18 SCARA manipulator and response plot.

Block diagram of realized position based local impedance control system is presented in Fig. 19 (K_P and K_D – proportional and derivative feedback gains respectively).

The second-order low-pass filter was implemented to eliminate noise component with cutoff frequency of 80 Hz.

V. Conclusion

New optical torque sensors in order to replace the strain-gage-based 6-axis force/torque sensor and realize virtual backdrivability of joint transmissions have been developed. These sensors are compact, light in weight, easy to manufacture, moreover, they have good linearity, enough resolution and electromagnetic noise immunity. Position based local impedance control of SCARA type manipulator has been successfully implemented. The new anthropomorphic arm with ability build in developed torque sensors has been designed. New stage of research is realization of the local impedance control of each joint of the robot arm.

References

[1] R. Tadakuma, Y. Asahara, H. Kajimoto, N. Kawakami, and S. Tachi: "Development of anthropomorphic multi-D.O.F. master-slave arm for mutual telexistence," *IEEE Transactions on Visualization and Computer Graphics*, vol. 11, no. 6, pp. 626-636, November 2005

[2] J. D. Turner and M. H. Westbrook, *Automotive Sensors*. Bristol, U.K.:IOP, 1993.

[3] P. L. Fulmek, F. Wandling, W. Zdiarsky, G. Brasseur, and S. P. Cermak, "Capacitive sensor for relative angle measurement, " *IEEE Transactions on Instrumentation and Measurement*, vol. 51, no. 6, pp. 1145-1149, December 2002.

[4] A. M. Madni, R. K. Hansen, and J. B. Vuong, "Differential capacitive torque sensor," U.S. Patent No. 6 772 646, 2004.

[5] S. Hirose and K. Yoneda, "Robotic sensors with photodetecting technology," *Proc. of 20th International Symposium on Industrial Robotics*, pp. 271-278, 1989.

[6] S. Hirose and K. Yoneda, "Development of optical 6-axial force sensor and its non-linear calibration," *J. of RSJ*, vol. 8-25, pp. 19-28, 1990.

[7] N. Okutani and K. Nakazawa, "Torsion angle detection apparatus and torque sensor," U. S. Patent No. 5 247 839, 1993.

[8] S. J. Horton, "Displacement and torque sensor," U. S. Patent No. 6 800 843 B2, 2004.

[9] Photointerrupter Design Guide. *Product catalog of ROHM*, pp. 6-7, 2005.

[10] M. M. Williamson, "Robot arm control exploiting natural dynamics," *PhD thesis*, Massachusetts Institute of Technology, 1999.

[11] C. Nicot, "Torque sensor for a turning shaft," U. S. Patent No. 6 694 828 B1, 2004.

[12] D. Vischer and O. Khatib, "Design and development of high-performance torque controlled joints," *IEEE Transactions on Robotic and Automation*, vol. 11, no. 4, pp. 537-544, August 1995.

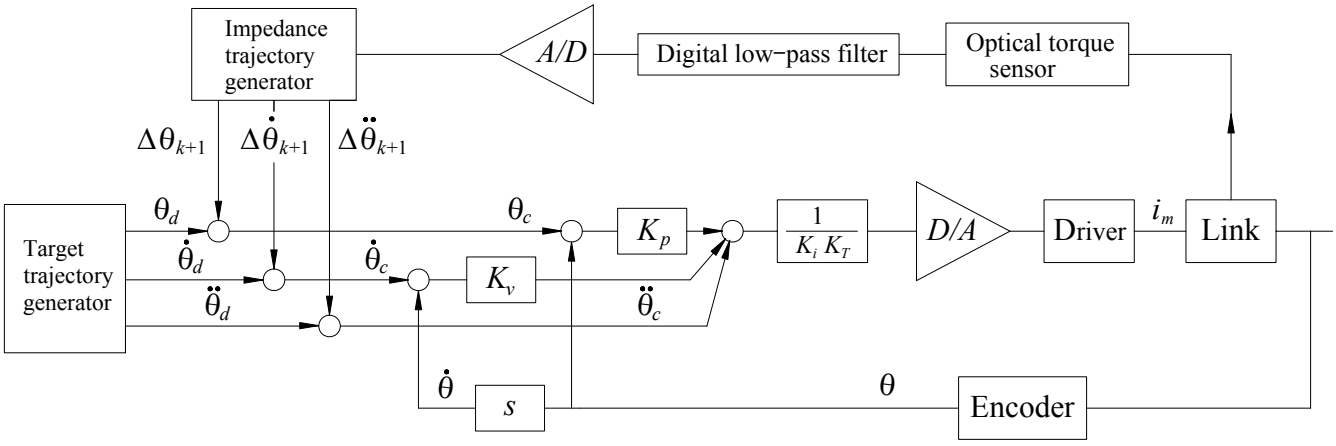

Fig. 19 Block diagram of the position based impedance control.